Exciton-polariton eigenmodes in light-coupled $In_{0.04}Ga_{0.96}As/GaAs$ semiconductor multiple-quantum-well periodic structures

J. P. Prineas, C. Ell, E. S. Lee, G. Khitrova, H. M. Gibbs, and S. W. Koch*
Optical Sciences Center, University of Arizona, Tucson, Arizona 85721
(Received 16 August 1999; revised manuscript received 21 December 1999)

Features of exciton-polariton eigenmodes in a series of light-coupled $In_{0.04}Ga_{0.96}As/GaAs$ semiconductor multiple quantum wells with varying number of quantum wells N from 1 to 100, and with various periodicities (Bragg, near-Bragg, and anti-Bragg), are studied in linear measurements of reflection, transmission, and absorption. At Bragg periodicity (period $d=\lambda_x/2$), a photonic band-gap mode grows in amplitude and increases linearly in linewidth with increasing N. The N times increased radiative damping rate is seen to arise from the light character of the eigenmode being swept out of a photonic band-gap structure. The slope of linewidth versus N gives the radiative linewidth of the exciton. Away from Bragg periodicity two branches of energy levels can be resolved in absorption, corresponding to the N exciton-polariton normal modes in the multiple-quantum-well structure. Signatures of individual modes becoming optically active are observed in the rich structure of reflection spectra for changing quantum-well periodicity. Antireflection coating of the samples is shown to be an effective way of thus isolating the multiple-quantum-well response.

I. INTRODUCTION

A topic of basic interest to semiconductor and solid-state physics is the study of the optical and electronic properties of layered and periodic structures. A wealth of high-quality layered structures such as optical microcavities, quantum-well (QW) embedded microcavities, superlattices, and multiple-quantum-well (MQW) nanostructures has been made possible by the development of epitaxial growth techniques such as molecular beam epitaxy (MBE) in the last few decades. Such structures have been used to tailor the optical and electronic properties of semiconductors and to investigate fundamental physical phenomena. In this study we report on features of N light-coupled QW's, or exciton-polariton eigenmodes, in MQW structures with N QW's spaced with Bragg and non-Bragg periodicities in linear measurements.

Building upon early works of radiative lifetime of excitons in QW's,[1–3] Ivchenko, Nesvizhskii, and Jorda[4] established the N times broadening of the radiative linewidth of the exciton-polariton mode at Bragg resonance, the so-called ''superradiance.'' This was confirmed and extended further.[5–12] The first observation of superradiance in the time domain in Bragg MQW's done in degenerate four wave mixing (DFWM) experiments on $GaAs/Al_xGa_{1-x}As$ QW's by Hübner *et al.*,[13,14] showed an N times enhanced decay rate of the excitonic polarization. The broadening was observed in the spectral domain in reflection in $CdTe/Cd_xMn_{1-x}Te$ (Ref. 15) and in $CdTe/Zn_xCd_{1-x}Te$ (Ref. 16). A direct analogy to Bragg MQW's in atomic systems is the N times increase of the radiative damping rate predicted in an optical lattice of atoms, formed by trapping atoms in a standing wave of light and probed with a weak linear probe.[17]

As we will show in this paper, in both situations, the fast decay, or spectral broadening, arises from the formation of a photonic band gap from the index contrast, not the absorption, at the dipole planes spaced with Bragg periodicity. Light is forbidden in such a structure and is swept out with an enhanced decay rate. The effect is basically the same as light reflected from a dielectric distributed Bragg mirror and shows some similarities but also pronounced differences to collective (superradiant) emission from atoms within a volume small compared to λ_{atom}.

Some of the most interesting radiative coupling effects are observed with the QW period that is different from the Bragg condition where $d=\lambda_x/2$, with d the center-to-center QW spacing, and λ_x the wavelength in the material corresponding to the $1s$ electron–heavy-hole (e-hh) exciton energy $E_x=hc/\lambda_x$. Separated by large enough barriers so that they are electronically uncoupled, the QW's are still coupled by light propagating in the MQW structure. Each QW is a complicated semiconductor crystal with quantum confinement in the growth direction and the potential for containing a very high density of excitons and carriers. Nonetheless from a linear-regime, radiative-coupling viewpoint, much can be learned by treating each QW as a single classical oscillator. Then N coupled oscillators result in N normal modes. For ideal QW's at exact Bragg spacing, only one mode, the superradiant mode, couples to the field. But away from Bragg spacing, all N modes couple to the field. Some are bright, that is, with stronger radiative damping, and some are dark or subradiant, with reduced radiative damping, giving rise to an energy ''band'' with N sublevels.

One particular period that has been investigated both theoretically and experimentally in the semiconductor case is the anti-Bragg periodicity, i.e., $d=\lambda_x/4$, where observation of an energetic splitting of the modes has been predicted[6,10,18] and observations have been reported[13] in polarization beats via DFWM experiments. A splitting has also been reported at a $\lambda_x/6$ periodicity.[19]

We began our study by growing a series of MQW Bragg structures with a much larger range of N (up to 100) and with a much larger range of periods d than previously available. The structures were studied in reflection (R), transmission (T), and absorption $A=1-R-T$ in the linear regime. Grow-

ing MQW's with varying N gave us the opportunity to test the prediction of a linear growth of the radiative damping rate with increasing N in reflection for Bragg MQW's. A way to determine the radiative contribution to the total exciton linewidth, which is made up of homogeneous (both radiative and nonradiative) and inhomogeneous parts, is also presented. By taking advantage of the wedge shape of the layers in our structures, we studied properties of the N eigenmodes as a function of QW periodicity, which all become coupled to the field away from Bragg periodicity to some degree, again in linear R, T, and A. These results can be successfully modeled by linear dispersion theory.

A technique to isolate the MQW response and remove the effect of the cladding layer (shown to influence the radiative properties of the collective system[16]) is developed that entails antireflection (AR) coating the sample on both the front and back.

II. THEORETICAL BACKGROUND

A. Eigenmodes in a MQW structure with arbitrary periodicity

Exciton-polariton modes were originally discussed by Hopfield[20] by diagonalizing the Hamiltonian for a bulk crystal interacting with the quantized modes of the electromagnetic field. Furthermore, it was realized that the exciton-polaritons correspond to resonances in the transmitted intensity. These two approaches have given rise to two techniques used to solve for the exciton-polariton modes in a MQW.[4–9] One approach solves for eigenmode energies and damping rates from resonances in some quantity characterizing the excitons[7] (material approach) or as resonances in some quantity characterizing the light propagation through the medium[4,5] (optical approach). In this paper we follow the optical approach: eigenmode energy and damping rates are solved by finding the complex poles in the transmission coefficient for the N periodic QW structure. The transmission coefficient for the structure is calculated using a transfer matrix approach, as discussed in Sec. II B. The real part gives the energy shift and the imaginary part gives the damping. In special cases, such as at the exact Bragg configuration, the transmission coefficient is an analytical expression, as discussed in Sec. II C, but in general, the complex poles must be solved numerically. The case of $N=60$ is shown for a limited range of barrier thicknesses around the Bragg condition in Fig. 1. Figure 1(a) displays the eigenenergies of the modes referenced to the 1s e-hh exciton energy E_x. At periodicities different from Bragg, the mode energies cluster around two branches, as can be seen in Fig. 1(a). Figure 1(b) shows the corresponding damping rates of the modes, which are also a measure of the potential coupling to the field. At Bragg periodicity, it is seen that the coupling of all modes to the field goes to zero except for the one superradiant mode. For further clarity, the eigenenergies and corresponding widths for two different periodicities, Bragg and 1.03 times the Bragg spacing, are shown above the exciton spectrum in Fig. 2.

B. Linear dispersion theory

Linear dispersion theory (LDT) has been highly successful in modeling measurements linear in R and T for Bragg MQW's[21] and other coupled structures such as atomic[22] and quantum-well embedded microcavities.[23] In this paper LDT, is used to model the R, T, and A on and off-Bragg resonance for our samples. LDT, based on a transfer matrix approach,[24,25] requires detailed knowledge of the absorption coefficient α and the index n, corresponding to the complex

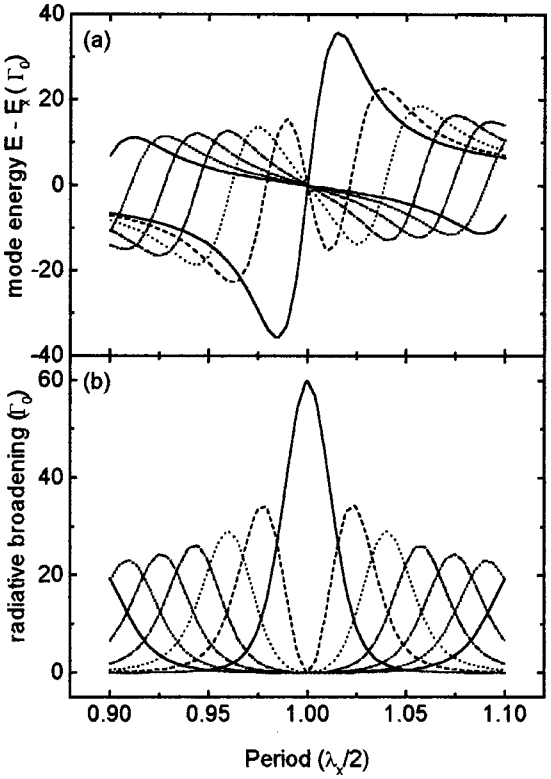

FIG. 1. (a) Calculated energy shifts (relative to the 1s e-hh exciton E_x) of the first six modes on both sides of Bragg periodicity for an $N=60$ MQW. At Bragg periodicity the N QW's are uncoupled and degenerate. Away from Bragg spacing, the radiative coupling splits the N normal modes of the system into a ''band'' with two subbranches. (b) shows the calculated radiative broadening of the first six modes around Bragg periodicity. At the Bragg spacing, $N-1$ modes are dark; only the superradiant mode is bright.

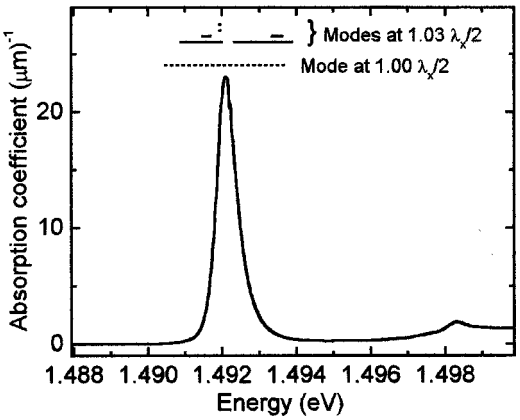

FIG. 2. Measured and extracted absorption coefficient for the $In_{0.04}Ga_{0.96}As/GaAs$ QW's in this study, used as input for LDT. Superimposed at the top are the calculated energetical position and widths of the eigenmodes from Fig. 1 for two QW periodicities, Bragg (dashed line) and 1.03 times the Bragg spacing (solid lines).

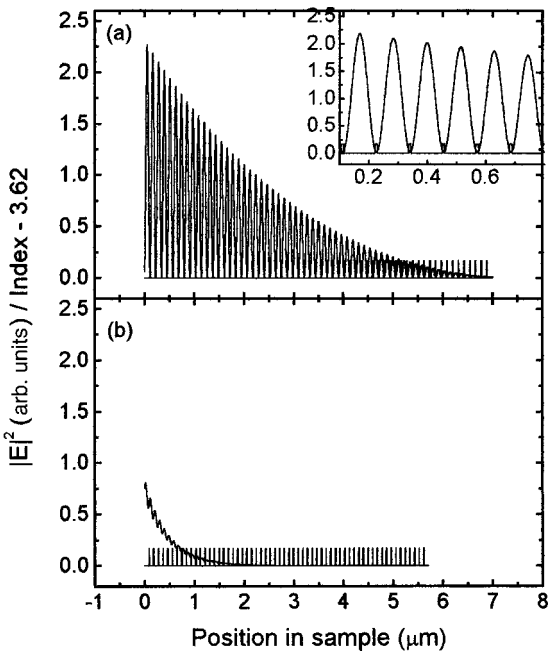

FIG. 3. (a) $|E|^2$ distribution, proportional to intensity distribution, in a 60-MQW structure at Bragg periodicity calculated by LDT for $\lambda = hc/E_x$. The inset is a closeup of a portion of (a) to clearly show that the field nodes occur at the QW's. (b) Same calculation as (a) except for $0.80\lambda_x/2$ periodicity.

dielectric response, in each layer. In contrast to Secs. II A and II C, where an idealized excitonic susceptibility is used to calculate the eigenmodes and to derive the analytical expressions, respectively, here the material input is measured, spatially averaged over the probe diameter. The measured absorption coefficient of the e-hh exciton and its continuum and higher states for our samples is shown in Fig. 2. The absorption coefficient was extracted from a transmission measurement of the $N=30$ MQW at a periodicity of $0.8\lambda_x/2$, where radiative coupling effects are less pronounced, using Beer's law: $\alpha=(1/N)\ln(I_0/I)$, where α is the absorption coefficient, N the number of QW's, I_0 the incident intensity, and I the transmitted intensity. The index was obtained from the absorption coefficient using a Kramers-Kronig transformation. The background dielectric response was assumed to be the same as that of the GaAs barrier, a good approximation due to the low concentration of In in our $In_{0.04}Ga_{0.96}As$ QW's. Further, making this assumption in LDT reproduces the measured T quite well. See Ref. 21 for a more detailed justification of this procedure.

LDT can also be used to construct the electromagnetic field and spatial intensity distributions in layered structures, including the MQW's considered here. For this calculation, each layer of the structure is artificially divided into slices, and the field is calculated in each slice. The intensity distribution in the steady-state spectral domain for 60 QW's at λ_x is calculated for Bragg and off-Bragg periods in an AR-coated sample in Fig. 3. Figure 3(a) shows that the QW's are located at the nodes of the field, in agreement with the result for an infinite number of QW's in Ref. 4. In our case, due to the finite well width and structure length, there is some small overlap of the field and the QW's, causing the standing wave to slowly decay through the structure. Away from the Bragg periodicity, the field quickly decays in the first part of the structure because the field cannot avoid the quantum wells and is thus quickly attenuated, as shown in Fig. 3(b).

C. Bragg resonance

Beginning from an exciton susceptibility with a single pole and no disorder as an input to the LDT calculation, an analytical expression for the transmission and reflection coefficients can be derived for MQW's with exact Bragg periodicity. The analytical expression conveniently illustrates the dependence of the collective response of the system as a function of the number of QW's N:[4]

$$\tilde{r}_N(kd=\pi)=\frac{-iN\Gamma_0}{\hbar\omega_0-\hbar\omega-i(\Gamma+N\Gamma_0)}, \tag{1}$$

$$\tilde{t}_N(kd=\pi)=(-1)^N\frac{\hbar\omega_0-\hbar\omega-\Gamma}{\hbar\omega_0-\hbar\omega-i(\Gamma+N\Gamma_0)}, \tag{2}$$

where $k=(\omega/c)n_b$ is the wave vector of light in the sample and is normal to the QW planes, n_b is barrier refractive index, d is the QW period, Γ is the nonradiative exciton damping rate of a single QW, Γ_0 is the radiative damping rate of a single QW, and ω_0 is the $1s$ heavy-hole exciton resonant frequency. Thus in a Bragg MQW, there is a single pole in the reflection and transmission coefficients corresponding to a superradiant mode with resonant frequency ω_0, Lorentzian shape, and total damping rate

$$\gamma=\Gamma+N\Gamma_0, \tag{3}$$

which has an N times enhanced radiative damping rate compared to a single quantum well (SQW).

The reflection amplitude for a MQW may be written

$$R=\left|\frac{r_{01}+\tilde{r}_N e^{2i\phi'}}{1+r_{01}\tilde{r}_N e^{2i\phi}}\right|^2, \tag{4}$$

where r_{01} is the reflection coefficient at the interface between vacuum and the outermost barrier layer, and ϕ' is the phase change a wave undergoes in traveling a distance $l-\pi/k$, where l is the thickness of the cladding layer. Hence the cladding layer masks the intrinsic radiative linewidth. In a Bragg MQW with the top layer of the same thickness as the barriers, or $l=\pi/k$, the reflection consists of a Lorentzian sitting on top of a background reflection $|r_{01}|^2$, with linewidth

$$\gamma=\Gamma+(1-r_{01})N\Gamma_0. \tag{5}$$

From a consideration of the dispersion relation it was pointed out[4] that in an infinite Bragg structure with ideal two-dimensional (2D) QW's, a standing wave forms in the structure such that the QW's are located at the nodes of the field. Hence the coupling of the excitons to the electromagnetic field is decreased at the Bragg resonance. The above results are tested experimentally in this paper.

III. EXPERIMENTAL METHOD

A. Samples

All samples were grown by MBE. The structures consist of 85-Å $In_{0.04}Ga_{0.96}As$ QW's with GaAs barriers grown on a semi-insulating GaAs substrate, and with a top cladding layer equal to the barrier thickness. The $In_{0.04}Ga_{0.96}As$ QW's are particularly well suited to this study, because the background dielectric responses of both the barrier and the low indium concentration $In_{0.04}Ga_{0.96}As$ QW's are the same, making it easier to concentrate on the pure excitonic effects. The strain introduced by the indium in the QW layer shifts the light-hole energy far above that of the heavy hole, further idealizing experimental conditions. The $In_{0.04}Ga_{0.96}As$ QW's also have the experimental advantage that the GaAs substrate is transparent in the energy range of the 1*s* QW exciton, making the structures convenient to study in transmission. MQW's were grown with $N=1$, 3, 10, 30, 60, and 100 QW's. The 1-, 3-, 10-, 30-, and 60-QW samples were grown under the same conditions close together in time. The 100-QW sample was grown some time later after some changes were made to the MBE machine, but was grown in the same way.

Because the flux maxima were directed to the center of the rotating substrate, all layers in the structure become monotonically thinner as a function of radius from growth center. Moving along a radius, the period decreases while the QW exciton energy stays essentially constant. Although the QW becomes thinner, its exciton energy does not change much because it is determined in first order by the 3D band gap, which is independent of QW thickness, and in second order by the confinement energy. Samples were grown so that Bragg periodicity typically occurred 1 to 2 cm from growth center, so then d could be swept through $\lambda_x/2$ by moving the probe along a radius from growth center.

A strip along a radius of the samples was given an AR coating on the front and back. The 1-, 3-, 10-, 30-, and 60-QW samples were AR coated with a single quarter-wave layer of material having index close to $(n_{GaAs})^{1/2}$ by CVI Corporation, and the 100-QW sample was AR coated in-house with a single quarter-wave layer of HfO_2 having also an index close to $(n_{GaAs})^{1/2}$. The AR coatings on bulk GaAs have a room-temperature reflectivity of about 0.2%, and a low-temperature reflectivity of about 0.75% from bulk GaAs. The role of the AR coating is to remove the influence of the cladding layer of the samples, as discussed in Sec. IV.

B. Method

Measurements of the linear reflectivity and transmission were done with a broad-band, square-wave-driven light-emitting diode (LED). Its output was first monochromatized with a 1.25-m scanning Spex spectrometer to a 0.35-Å band pass, to produce a very weak 100-pW monochromatic probe, which was imaged to a 50-μm diameter spot on the sample, with an f number of 12. The monochromatized probe was detected by a fiber-coupled Hamamatsu H943-02 photomultiplier tube, and amplified with a Stanford Research Systems DSP 830 lock-in amplifier. The samples were cooled to 8 K by a helium closed-cycle APD cryogenics cold finger. All measurements were done with the above setup except the measurement of the reflection of the 100 MQW versus periodicity, which was done in an open-cycle helium cold finger at 4 K, with weak 100-fs pulses with average power 0.1 μW, focused to 50 μm. The signal was resolved by a 32-cm Princeton Instruments (PI) spectrometer with a 0.6-Å band pass and detected by a PI liquid-nitrogen-cooled charge-coupled device (CCD) array.

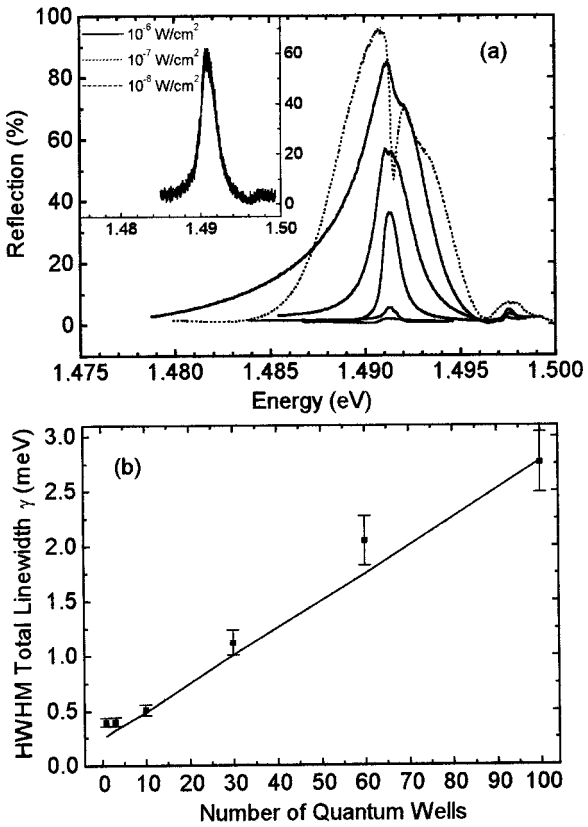

FIG. 4. (a) Increase of experimental reflection with N for 1, 3, 10, 30, 60, and 100 QW's with Bragg periodicity. The experimental measurements were done with an AR coating on the front and back. (b) Square dots with error bars represent experimental HWHM linewidths for AR-coated samples measured in reflection. The solid line is generated from LDT for MQW samples in semi-infinite GaAs using the measured QW absorption coefficient. It is a straight line with slope $\Gamma_0=27\pm2$ μeV, where Γ_0 is the HWHM radiative width. The inset to (a) shows reflection from a 30-MQW Bragg structure in the limit of vanishing exciton density, emphasizing that the superradiance phenomenon does not depend on exciton density.

IV. EXPERIMENTAL RESULTS AND DISCUSSION

A. MQW's with Bragg spacing

The principal experimental result at Bragg periodicity is the growth of a photonic band gap in reflection, growing in amplitude and in linewidth with N, as can be seen in Figs. 4 and 5, the so-called superradiant response. Figure 4(b) conclusively shows that experimentally the linewidth in reflection for the collective system does indeed increase linearly with N, at least for AR-coated structures, in accordance with Eq. (3). Thus Eq. (3) allows a convenient way to extract the radiative linewidth from the slope of linewidth versus N and the remaining contributions to the linewidth from the intercept. Such an extraction yields a least-squares value of 27 ±2 μeV for the half width at half maximum (HWHM) ra-

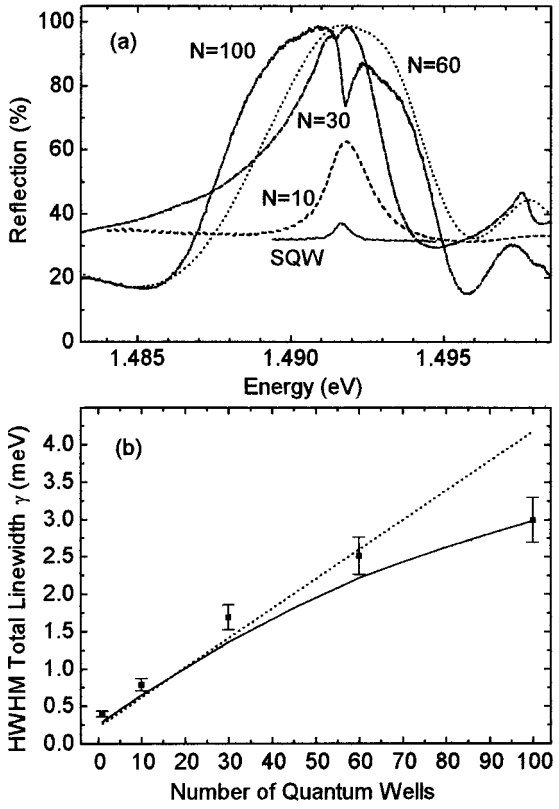

FIG. 5. (a) Experimental reflection from MQW's, 1-, 10-, 30-, 60-, and 100-QW, samples with Bragg periodicities and Bragg cladding layers and no AR coating. (b) Square dots with error bars represent experimental HWHM linewidths for samples with a Bragg cladding layer and no AR coating measured in reflection. The solid line is generated from LDT for the experimental MQW structures. The dotted line is a plot for MQW's with a Bragg cladding layer and no AR coating as predicted by Eq. (5), using the value for Γ_0 experimentally obtained from Fig. 4(b).

diative width and 0.32 ± 0.03 meV HWHM for the remaining nonradiative and inhomogeneous contributions of our $In_{0.04}Ga_{0.96}As$ QW's. Γ_0 can also be determined by precision reflection measurements from a single quantum well as shown in Ref. 26. However, the method in our work has much larger signals. The variation in the quantum wells of a MQW sample is expected to have very little effect on Γ_0, since it depends mostly on the well material and thickness.

Figure 6(a) shows that LDT reproduces the measured *R*, *T*, and *A* at Bragg periodicity. LDT even reproduces the measured line shapes. The asymmetry of the reflection line shapes in Fig. 4(b) for large *N* and deviation from a Lorentzian shape are due to the influence of higher states such as the $2s$ and continuum states, whereas Eqs. (1)–(5) assume a single-exciton resonance approximation. We verified that the asymmetry for large *N* is reproduced by our theory even when an excitonic susceptibility with a homogenous Lorentzian line shape is used, indicating that the asymmetry results from the contributions of the $2s$ and higher states and not from disorder. Finally, we have demonstrated that it is possible to determine the radiative contribution to the linewidth from the measured absorption coefficient alone using LDT as an extraction tool by generating a plot of linewidth versus *N* and finding the slope.

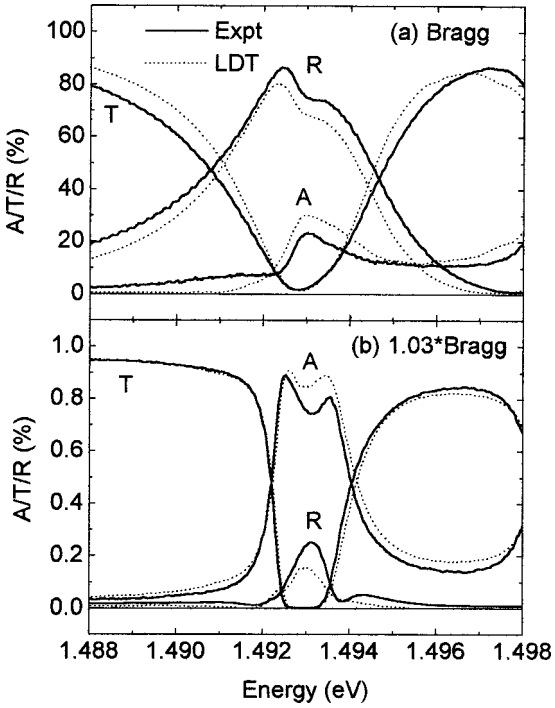

FIG. 6. (a) and (b) show the measured *R*, *T*, and *A* at Bragg periodicity (solid lines) and 1.03 times Bragg periodicity, respectively, and corresponding *R*, *T*, and *A* calculated by LDT (dashed lines) for $N = 60$.

One difference between experiment and the theoretical assumptions used for Eqs. (1)–(5) is the presence of inhomogeneous broadening. From other measurements,[27] it is known that the nonradiative contribution to the homogeneous width is not much larger than the radiative contribution obtained above; hence the linewidths are inhomogeneously broadened by a factor of roughly 5 in the case of our $In_{0.04}Ga_{0.96}As$ SQW. In previous theoretical papers, the lines were assumed to be homogeneously broadened. For the small absolute inhomogeneous broadening in these samples, it is a good approximation to simply lump the inhomogeneous broadening with the nonradiative homogenous broadening in Eq. (3), so that $\Gamma = \Gamma_{\text{inh}} + \Gamma_{\text{nonradiative}}$. Inhomogeneous broadening basically causes the various oscillators to become slightly detuned from one another. The inhomogeneous broadening in these samples corresponds to averaging over periodicities with such minute differences from Bragg $[(1.0000 + - 0.0001)\lambda_x/2]$ as to be insignificant. Therefore the inhomogeneous broadening acts only as the intercept to the linear dependence of linewidth on *N*, Eq. (3). Such a simplification would not be true if, for example, the inhomogeneous broadening were much larger, or *N* was much higher, where the modes become more closely spaced for changing QW periodicity. In that case light could couple to the other modes, and coupling to the photonic band-gap mode could be significantly decreased. One final note on the subject of linewidths is that for MQW's with large *N*, the linewidths are by far predominantly radiatively broadened at Bragg periodicity, i.e., $N\Gamma_0 \gg \Gamma_{\text{inh}}$.

An ideal AR coating removes the effect of the cladding layer and mimics an MQW structure embedded in semi-infinite GaAs. The principal evidence for this is that the am-

plitude, linewidth, and the line shape of *R*, *T*, and *A* spectra generated by LDT assuming the MQW was embedded in semi-infinite GaAs agree very well with the experimental *R*, *T*, and *A* measurements of the AR-coated samples, as shown in Fig. 6. Besides isolating the pure MQW response, the AR coating may have the practical application of increasing the efficiency and contrast of a Bragg optical switch[14] by increasing the amount of light getting into the structure and decreasing the background reflection.

Without an AR coating, the cladding layer plays an important role in influencing the radiative damping[11,16] seen in reflection measurements. For $N=30$, the cladding increases the damping rate by a factor of as much as 1.5. A comparison of Figs. 4(b) and 5(b) shows the experimental difference in linewidth between samples with and without an AR coating. In contrast to Eq. (5) (r_{01} is negative for the $\lambda_x/2$ cladding layer) and shown in Fig. 5(b) (dotted line), the dependence is not simply linear with an increased slope, but curved, and begins to level off for large *N*. LDT reproduces this behavior, also shown in Fig. 5(b) (solid line). The reason for this deviation is that the $\lambda_x/2$ cladding layer strongly increases the amplitude of the reflection, causing it to ''saturate,'' i.e., *R* cannot increase above 1. Therefore the spectral shape of *R* must deviate from a Lorentzian and become more square, as shown in Fig. 5(a). Such a saturation was also calculated for atoms in an optical lattice.[17] Already by $N=30$ QW's, the reflectivity is nearly 100%, while in an AR-coated structure we expect $N\approx 200$ is needed to produce this effect. Reexamination of Fig. 5(b) shows that Eq. (5) in fact agrees with experiment and LDT for small *N*, before ''saturation'' is reached.

One interesting question is whether a cladding layer can influence the linewidth of a SQW. While in theory it can, we did not observe any difference in linewidth within experimental error. In a SQW, because the radiative linewidth is only 10% of the total linewidth, as shown above, even changes of a factor of 1.5 in the radiative linewidth make only small changes in the total linewidth. The ratio of the peak absorption *A* at the exciton resonance for no AR divided by that with an AR was approximately $\frac{2}{3}$. This is due to the trivial effect of $\frac{2}{3}$ less light getting into a non-AR-coated sample compared to an AR-coated sample. It is possible that the ratio is smaller than this, based on the field distribution, but again it was not observable within experimental error. The situation would be different if the radiative component made up a larger portion of the total linewidth.

At Bragg spacing, the exciton-polariton is more lightlike in character than at any other periodicity, and the exciton character is diminished. As shown in Fig. 3(a), the field is nearly zero at the QW's. Experimental evidence of the field distribution shown in Fig. 3(a) can be seen in transmission: In spite of the reflection reaching a maximum at Bragg periodicity in the 60-MQW structure, as shown experimentally in Fig. 7(d), the light transmitted by the structure is at a maximum at Bragg periodicity, as shown in Fig. 7(c). Compare Figs. 6(a) and 6(b) for an alternative representation of the data. The maxima in *R* and *T* at Bragg resonance correspond to a minimum in absorption, shown in Fig. 7(a). While the energy stored in the QW's is at a minimum, the energy stored in the electromagnetic field is at a maximum at Bragg resonance, as shown in Fig. 3, which shows the intensity

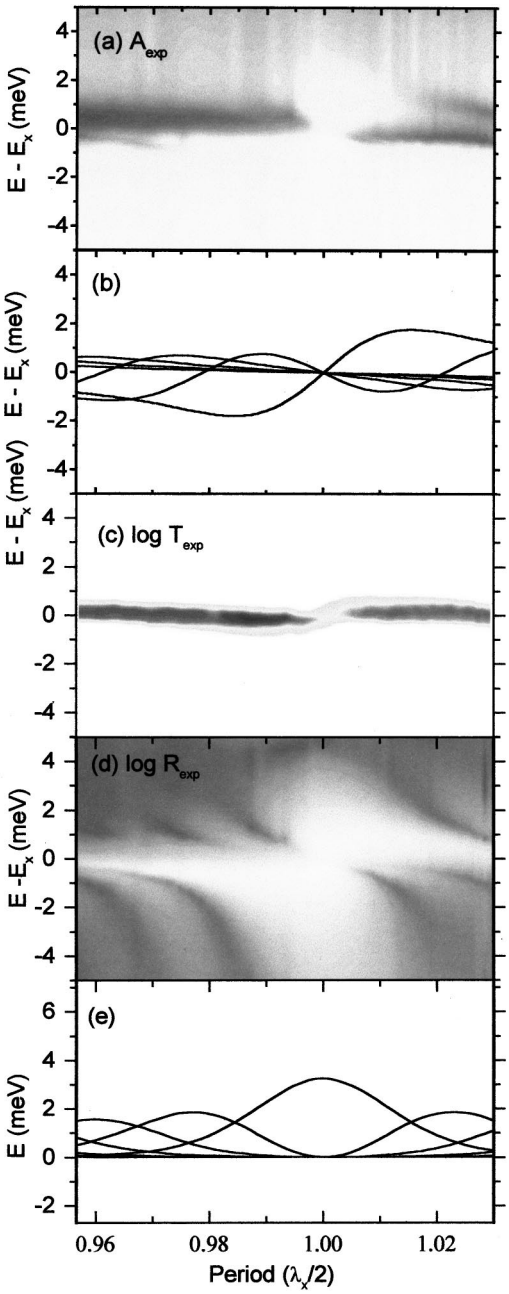

FIG. 7. (a) Experimental absorption for a 60-MQW structure. The shade becomes darker for larger absorption. (b) Calculated energy shifts of the exciton-polariton modes in a 60-MQW structure for comparison to experiment. The splitting observed experimentally agrees with the calculated energetical positions of the modes. A minimum in absorption is seen to occur in (a) at Bragg periodicity. (c) and (d) show the logarithm of the corresponding experimental transmission and reflection, respectively. Maximum in both transmission and reflection occur at Bragg periodicity. The shade becomes whiter for larger reflection and transmission. (e) shows the calculated damping rates (FWHM) of the eigenmodes for comparison to (d).

distribution, in the same relative units for Bragg periodicity and 0.8 Bragg periodicity. The energy stored as light, found by integrating over the intensity distribution in the structure (e.g., as in Fig. 3), is 20 times greater at $d=\lambda_x/2$ than at $1.03(\lambda_x/2)$, and 60 times greater than at $0.8(\lambda_x/2)$ for the $N=60$ MQW.

The linear increase in the linewidth, or damping rate, with N can be understood from the point of view of light travelling in a Bragg periodic potential. Common to any situation of a wave traveling in a Bragg periodic potential, an energy gap forms at the boundary of the first Brillouin zone. For a light wave, a ''photonic band gap'' forms. Because propagating modes are forbidden in the band gap, they experience large damping, and the light is reflected out of the structure with an N times enhanced decay rate. The large mode damping may be viewed as the source of the ''superradiance.''

The superradiance discussed here can be compared/contrasted with the atomic situation. The Bragg resonance in monolithic semiconductor MQW's is most analogous to the situation of reflection of a weak probe from an optical lattice of atoms.[17] In the atomic case, the atoms are arranged in a lattice by a nearly resonant optical standing wave, positioning them with Bragg spacing. Theory has shown for increasing N planes of atoms, a large broad reflection signal grows as a Lorentzian, eventually turning into a square stop band with a fixed bandwidth for further increase of N. It was noted that even if the imaginary part of the dielectric function is artificially set to zero in the theory, the stop band essentially remains; in other words, the response is essentially an index effect. Thus the form of superradiance associated with photonic band gaps is more closely associated with the large damping experienced by the photon. It would perhaps be clearer to call the superradiant mode the photonic band-gap mode instead.

The photonic band-gap mode is quite different from atomic superfluorescence. Whereas superfluorescence times become shorter inversely with the number of excited atoms, the photonic band-gap mode discussed here depends only on the number of QW's and not on the excitation density within them (as long as the exciton susceptibility remains unchanged; but compare, e.g., Refs. 11 and 12 for intricate intensity-dependent effects). For example, the N times broadening is unchanged as the intensity of the monochromatized probe is weakened from 10^{-6} to 10^{-8} W/cm^2, i.e., in the limit of vanishing exciton density, as shown in the inset of Fig. 4 for the 30-QW structure.

B. MQW with non-Bragg spacings

Away from the Bragg resonance, the phenomena observable in MQW systems become even richer. While at Bragg resonance only the photonic band-gap mode is optically active, for periods different from Bragg, all the $N-1$ modes become optically active to some degree. It is convenient to view the eigenenergies from the QW point of view: At Bragg resonance, the index contrast between the barriers and QW's sets up a light field that is almost zero at the QW's, and the N QW oscillators are barely coupled. The Bragg MQW then consists of N degenerate energy levels, as shown in Fig. 1(a), as one would expect for N uncoupled oscillators. For other periods, the radiative coupling splits the degenerate QW oscillators into N sublevels accumulating around two energy branches. Direct evidence of the formation of split energy branches of the eigenmodes of the interacting system can be seen in Fig. 7(a) in absorption. The modes in each branch cannot be resolved, but the branches themselves can. The splitting is more distinct on the thicker side than the thinner side of the QW structure probably due to the asymmetry of the absorption coefficient, shown in Fig. 2: The sharper edge on the low-energy side, emphasized for periodicities thicker than Bragg, gives rise to sharper features of the collective system.

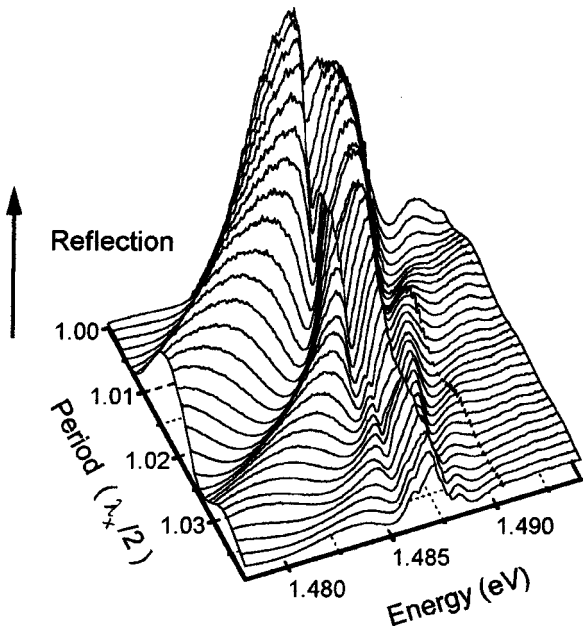

FIG. 8. Normalized experimental reflection from a 100-MQW structure, showing a rich behavior of peaks and dips peeling off as a function of periodicity.

In addition to absorption, signatures of the modes can also be seen in reflection. For example, see Figs. 7(d) and 8. Figure 7(d) shows the reflection from a 60-MQW as a function of periodicity. Peaks and dips are seen peeling off for periods different from the Bragg spacing. As Bragg spacing is approached, the bright photonic band-gap mode dominates the spectrum. Figure 8 shows a rather spectacular behavior in reflection from a 100-MQW structure as peaks and dips grow in the center of the spectrum and peel off for periods larger than the Bragg spacing as various modes become optically active. However, some care should be given to the interpretation of the dips and peaks in reflection; there is no simple one-to-one correspondence between a peak or a dip and a particular mode. Only the photonic band-gap mode at the Bragg condition can be identified as a peak. A numerical analysis using an ideal excitonic susceptibility with a Lorentzian broadening of 0.21 meV HWHM reveals that some of the reflection dips can be attributed to energetic mode positions. For example, Fig. 9 shows the calculated reflection spectra for the period $d=1.0065\lambda_x/2$ and $d=1.013\lambda_x/2$, and for two different SQW oscillator strengths. Since the energetic mode position, when scaled to Γ_0, is independent of the oscillator strength, only energetically overlaying reflection dips can be attributed to eigenmodes. Only these reflection dips agree energetically with peaks in the absorption (not shown here). Figure 9(a) and the inset in Fig. 9(b) show that as soon as the mode labeled 2 reaches its energetic minimum, the reflection dip starts to pull off to lower energies, so it is no longer a clear identification signature of an eigenmode energy. In Figs. 7(d) and 8, the photonic band-gap mode at the Bragg condition is a peak for all periodicities; the dips appearing as the periodicity increases or decreases

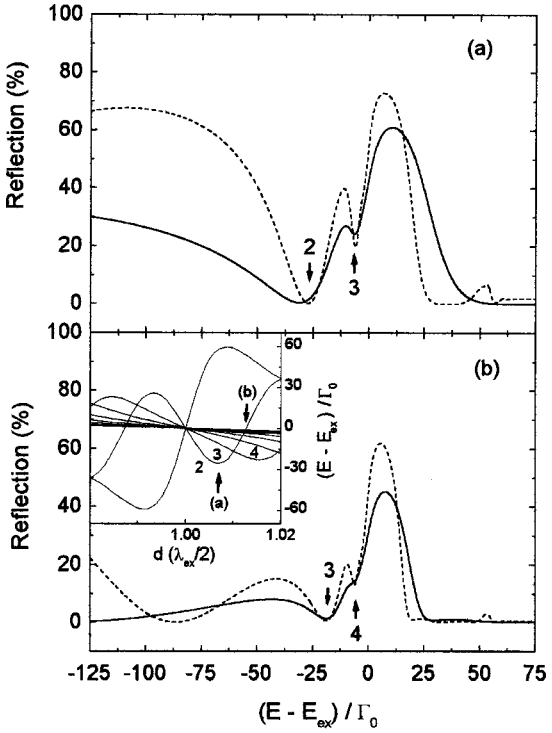

FIG. 9. Calculated reflection spectra of a 100 MQW at a period of (a) $1.0065\lambda_x/2$ and (b) $1.013\lambda_x/2$ for an oscillator strength proportional to Γ_0 (solid) and twice as large (dashed). The inset shows the real parts of the eigenmodes. The arrows show the corresponding mode numbers.

are at first associated with an individual mode. As the dip continues to peel off, it loses its mode identity.

This analysis shows that it is difficult to interpret reflection data of periodic MQW's. For example, one cannot simply identify reflection peaks with ''bright'' modes (modes with a radiative damping larger than Γ_0) as was done in Ref. 28. Kavokin and co-workers[28,29] found a narrowing of the reflection peak of a 5-QW sample compared to a SQW sample. They interpreted this behavior as a motional narrowing due to the underlying disorder. Figure 10 shows the calculated HWHM of the reflection peaks as a function of the

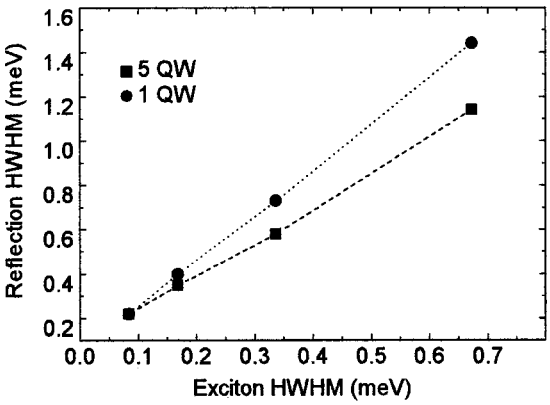

FIG. 10. Reflection peak linewidth as a function of the homogeneously broadened exciton linewidth for the sample characteristics of Baumberg *et al.* (Ref. 29) and Kavokin and Baumberg (Ref. 28).

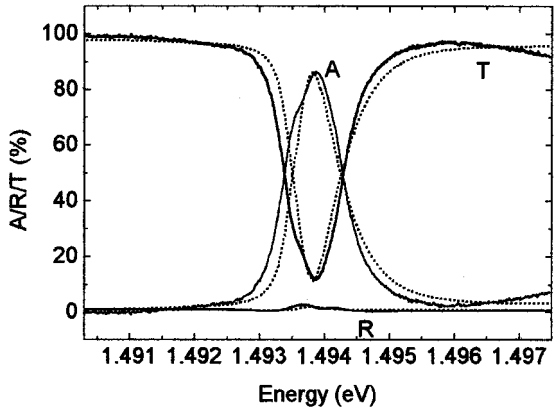

FIG. 11. The solid lines show the experimental absorption A, transmission T, and reflection R for an $N=10$ anti-Bragg structure. The dotted lines show the LDT calculation.

homogeneously broadened SQW exciton linewidth, i.e., one can reproduce the narrowing of the reflection peaks without any disorder.

The mode energetic positions are best interpreted in absorption as shown in Figs. 7(a) and 7(b) for $N=60$ QW's. The peaks in absorption coincide with the calculated mode energies. The success of LDT in explaining the reflection at all periods, at Bragg and away from Bragg periodicity, seen in Figs. 6(a) and 6(b), is excellent as expected.[21]

C. Anti-Bragg periodicity

In previous studies, a good deal of attention has been given to the anti-Bragg periodicity $d=\lambda_x/4$. Common to all periodicities except Bragg, all N coupled modes are optically active to varying degrees (i.e., several modes are brightest and dominate over the darker modes). Anti-Bragg periodicity was somewhat of a focus initially because a splitting of the absorption was predicted for that periodicity, which stands in contrast to the special case of Bragg periodicity. But in fact, the splitting of the N modes into two branches occurs at almost all periods (except Bragg), as is shown clearly in the absorption measurements shown in Fig. 7(a) for a small range of periodicities.

Anti-Bragg periodicity is unique only in that at (or near) that periodicity, light reflected from adjacent QW's destructively interferes. This makes anti-Bragg structures somewhat difficult to study from an experimental point of view because the reflected light signal is exceedingly small. Figures 11 and 12(a) show experimental reflection, as well as transmission and absorption, for $N=10$ and 30 AR-coated anti-Bragg structures, respectively. Superimposed is the calculation from LDT. A splitting is not resolved in absorption for either the experimental or the calculated spectra for these samples. Splitting is not resolved in LDT calculations using the measured absorption coefficient for anti-Bragg samples with N as high as 200. This is partly because the splitting decreases to its minimum value at $d=\lambda_x/4$. This minimum in splitting reaches a constant value in the limit of large N and becomes similar in character to the longitudinal-transverse splitting[6] of bulk. The magnitude and therefore the resolvability of the splitting at $d=\lambda_x/4$ depend more on the exciton linewidth than on the number of QW's N.

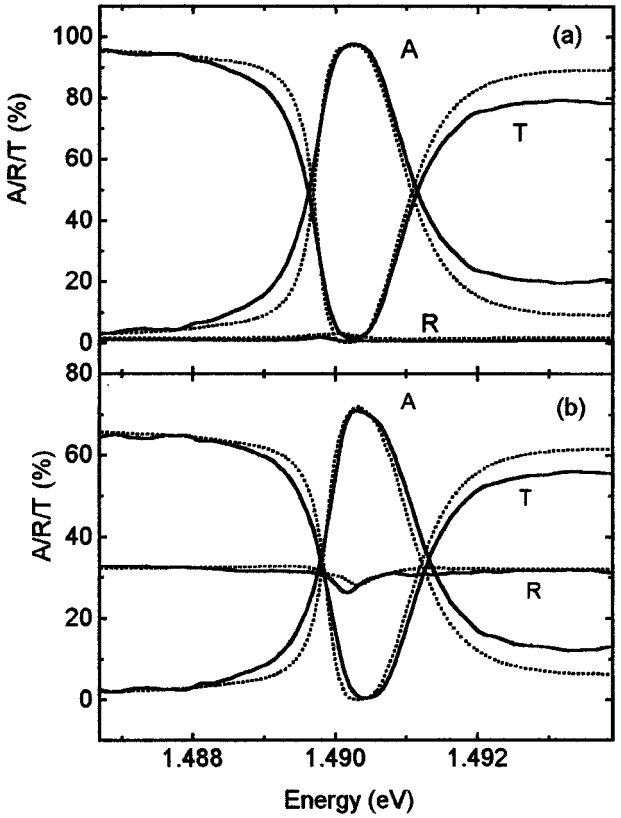

FIG. 12. The solid lines show the experimental absorption A, transmission T, and reflection R for an $N=30$ anti-Bragg structure. The dotted lines show LDT. (a) is for an AR-coated structure with an anti-Bragg cladding layer, while (b) is for the same sample but without an AR coating.

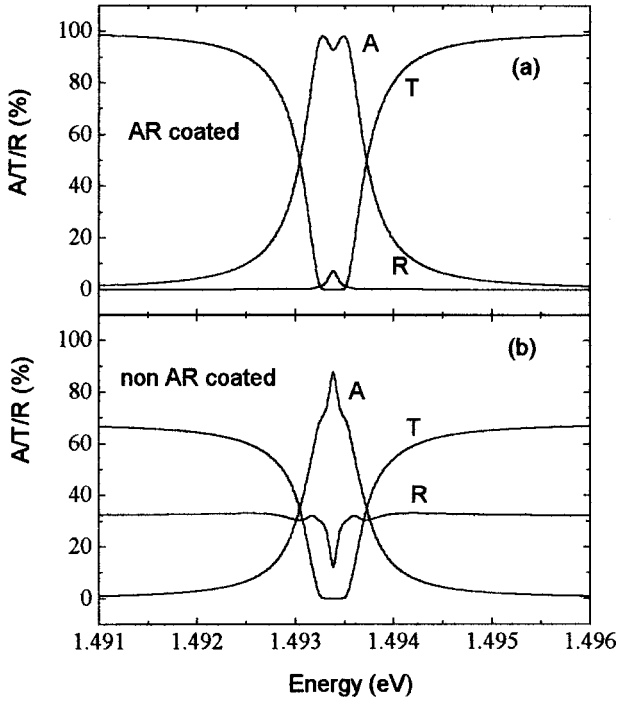

FIG. 13. (a) Calculated absorption A, transmission T, and reflection R for a sample with a perfect AR coating and a 5 times narrower linewidth than our experimental samples as a guide for understanding. (b) Same calculation with an anti-Bragg cladding layer and no AR coating.

The cladding layer on anti-Bragg structures can determine the absorption properties. To get a clearer picture of what to expect, an anti-Bragg structure, with 10 QW's and 5 times narrower, nonradiatively broadened line of 0.1 meV but approximately with the same oscillator strength and therefore radiative width, was numerically calculated. The calculated homogeneously broadened excitonic susceptibility was used as input into the LDT calculation as before. Figure 13(a) shows an anti-Bragg structure with a perfect AR coating. For this situation, there is a single dip in T, a single peak in R, and a splitting in A. However, if the structure is not AR coated, the reflection becomes a dip, and the absorption does not show splitting, but a larger peak, as can be seen in Fig. 13(b). This emphasizes the importance of AR coating samples to remove the influence of the cladding layer and to isolate the response of the MQW structure. It also shows that the resolvability of the splitting at anti-Bragg is quite sensitive to linewidth of the absorption coefficient.

The basic behavior of the structure with versus without the AR coating is illustrated experimentally in Fig. 12 for an $N=30$ MQW anti-Bragg structure with and without an AR coating. It is seen that without the AR coating, the reflection is a dip, whereas with an AR coating, the reflection becomes a peak. The splitting in absorption can still not be resolved. LDT reproduces the behavior well, although the peak in the experimental reflection is larger than that in LDT. This is because the AR coating in the LDT is perfect, whereas on the sample the surface still reflects about 0.75%. Since the modeled peak in reflection is about 0.3%, it can be assumed that the influence of the first interface has not been completely removed, and leads to the deviation between LDT and experiment.

As a final note, in the $N=10$ anti-Bragg structure, a small splitting, or shoulder, was observed in transmission not only for the $N=10$ sample shown here, but for several others, although not for the $N=30$. This shoulder in transmission was not reproduced by LDT, and is therefore speculated to be caused either by greater disorder in the anti-Bragg samples or greater influence of the disorder.

V. CONCLUSION

Linear reflection, transmission, and absorption reproduce in detail the analytical expressions, in particular the linear increase of radiative damping rate with increasing N of QW's, and the location of the intensity nodes at the QW's in Bragg MQW's. The exciton radiative lifetime was extracted from an experimental plot of linewidth versus N, and even from the line shape and magnitude of the absorption coefficient in conjunction with LDT to generate a plot of linewidth versus N. Exactly at Bragg periodicity, the light character is at a maximum, and the fast decay can be understood from the point of view of light being swept out of a photonic band-gap structure. Away from Bragg periodicity, the energy levels due to N radiatively coupled nearly identical QW's split into two branches; these were observed in measurements of the absorption. Although difficult to interpret, reflection spectra showed rich signatures of the N normal modes becoming optically active. A splitting was not resolvable in absorption for the anti-Bragg structures used in this

study. An AR coating was seen to be essential for removing the influence of the cladding layer and isolating the MQW optical response.

ACKNOWLEDGMENTS

The authors would like to thank DARPA/AFOSR; NSF AMOP, EPDT, LWT, and DMR; DARPA/ARO, JSOP (AFOSR and ARO); and COEDIP for support. J.P.P. thanks AASERT, C.E. the DFG (Germany), and H.M.G. the Humboldt Research Award for partial support. S.W.K. thanks the DFG (Germany) for support through the Sonderforschungsbereich 383 and the Leibniz program. We would also like to acknowledge fruitful discussions with Dr. J. Kuhl at the MPI in Stuttgart, Germany.

*Permanent address: Physics Department and Material Sciences Center, Philipps-University Marburg, Renthof 5, 35032 Marburg, Germany.

[1] L. C. Andreani, Solid State Commun. **77**, 641 (1991).
[2] D. S. Citrin, Solid State Commun. **84**, 281 (1992).
[3] E. L. Ivchenko, Fiz. Tverd. Tela (Leningrad) **33**, 2388 (1991) [Sov. Phys. Solid State **33**, 1344 (1991)].
[4] E. L. Ivchenko, A. I. Nesvizhskii, and S. Jorda, Fiz. Tverd. Tela (St. Petersburg) **36**, 2118 (1994) [Phys. Solid State **36**, 1156 (1994)].
[5] L. C. Andreani, Phys. Lett. A **192**, 99 (1994).
[6] L. C. Andreani, Phys. Status Solidi B **188**, 29 (1995).
[7] D. S. Citrin, Phys. Rev. B **49**, 1943 (1994).
[8] D. S. Citrin, Solid State Commun. **89**, 139 (1994).
[9] D. S. Citrin, Phys. Status Solidi B **188**, 43 (1995).
[10] T. Stroucken, A. Knorr, P. Thomas, and S. W. Koch, Phys. Rev. B **53**, 2026 (1996).
[11] S. Haas, T. Stroucken, M. Hübner, J. Kuhl, B. Grote, A. Knorr, F. Jahnke, S. W. Koch, R. Hey, and K. Ploog, Phys. Rev. B **57**, 14 860 (1998).
[12] T. Stroucken, S. Haas, B. Grote, S. W. Koch, M. Hübner, D. Ammerlahn, and J. Kuhl, Adv. Solid State Phys. **38**, 266 (1999).
[13] M. Hübner, J. Kuhl, T. Stroucken, A. Knorr, S. W. Koch, R. Hey, and K. Ploog, Phys. Rev. Lett. **76**, 4199 (1996).
[14] M. Hübner, J. Kuhl, S. Haas, T. Stroucken, S. W. Koch, R. Hey, and K. Ploog, Solid State Commun. **105**, 105 (1998).
[15] V. P. Kochereshko, G. R. Pozina, E. L. Ivchenko, D. R. Yakovlev, A. Waag, W. Ossau, G. Landwehr, R. Hellmann, and E. O. Göbel, Superlattices Microstruct. **15**, 471 (1994).
[16] Y. Merle d'Aubign, A. Wasiela, H. Mariette, and T. Dietl, Phys. Rev. B **54**, 14 003 (1996).
[17] I. H. Deutsch, R. J. C. Spreeuw, S. L. Rolston, and W. D. Phillips, Phys. Rev. A **52**, 1394 (1995).
[18] M. R. Vladimirova, E. L. Ivchenko, and A. V. Kavokin, Fiz. Tekh. Poluprovodn. **32**, 101 (1998) [Semiconductors **32**, 90 (1998)].
[19] M. Opher-Lipson, E. Cohen, and L. N. Pfeiffer, Phys. Rev. B **55**, 13 778 (1997).
[20] J. J. Hopfield, Phys. Rev. **112**, 1555 (1958).
[21] C. Ell, J. Prineas, T. R. Nelson, Jr., S. Park, H. M. Gibbs, G. Khitrova, S. W. Koch, and R. Houdr, Phys. Rev. Lett. **80**, 4795 (1998).
[22] Y. Zhu, D. J. Gauthier, S. E. Morin, Q. Wu, H. J. Carmichael, and T. W. Mossberg, Phys. Rev. Lett. **64**, 2499 (1990).
[23] G. Khitrova, H. M. Gibbs, F. Jahnke, M. Kira, and S. W. Koch, Rev. Mod. Phys. **71**, 1591 (1999).
[24] See, e.g., H. A. Macleod, *Thin-Film Optical Filters* (Elsevier, New York, 1969).
[25] L. A. Coldren and S. W. Corzine, *Diode Lasers and Photonic Integrated Circuits* (Wiley, New York, 1995).
[26] E. L. Ivchenko, P. S. Kop'ev, V. P. Kochereshko, I. N. Ural'tsev, D. R. Yakovlev, S. V. Ivanov, B. Ya. Mel'tser, and M. A. Kalitievski, Fiz. Tekh. Poluprovodn. **22**, 784 (1988) [Sov. Phys. Semicond. **22**, 495 (1988)].
[27] J. Kuhl, M. Hübner, D. Ammerlahn, T. Stroucken, B. Grote, S. Haas, S. W. Koch, G. Khitrova, H. M. Gibbs, R. Hey, and K. Ploog, Adv. Solid State Phys. **38**, 281 (1999).
[28] A. V. Kavokin and J. J. Baumberg, Phys. Rev. B **57**, R12 697 (1998).
[29] J. J. Baumberg, A. P. Heberle, A. V. Kavokin, M. R. Vladimirova, and K. Khler, Phys. Rev. Lett. **80**, 3567 (1998).